

# A Dynamic Mathematical Model of Bile Acid Clearance in HepaRG Cells

Daniel Kaschek,<sup>\*</sup> Ahmad Sharanek,<sup>†,‡</sup> André Guillouzo,<sup>†,‡</sup> Jens Timmer,<sup>\*,§,¶,1</sup> and Richard J. Weaver<sup>||,2</sup>

<sup>\*</sup>Institute of Physics, Freiburg University, Freiburg, Germany; <sup>†</sup>Inserm UMR 991 Foie, Métabolismes et Cancer, Rennes, France; <sup>‡</sup>Université Rennes 1, Rennes, France; <sup>§</sup>BIOSS Centre for Biological Signalling Studies, Freiburg, Germany; <sup>¶</sup>Freiburg Center for Systems Biology, Freiburg, Germany; and <sup>||</sup>Institute de Recherches Internationales Servier, Suresnes, France

<sup>1</sup>To whom correspondence should be addressed at E-mail: jeti@fdm.uni-freiburg.de.

<sup>2</sup>Institute de Recherches Internationales Servier, 50 Rue Carnot 922844 Suresnes, Cedex, France. Fax +33-155-725-40. E-mail: richard.weaver@servier.com.

## ABSTRACT

A dynamic model based on ordinary differential equations that describes uptake, basolateral and canalicular export of taurocholic acid (TCA) in human HepaRG cells is presented. The highly reproducible inter-assay experimental data were used to reliably estimate model parameters. Primary human hepatocytes were similarly evaluated to establish a mathematical model, but with notably higher inter-assay differences in TCA clearance and bile canaliculi dynamics. By use of the HepaRG cell line, the simultaneous TCA clearance associated to basolateral uptake, canalicular and sinusoidal efflux, was predicted. The mathematical model accurately reproduced the dose-dependent inhibition of TCA clearance in the presence and absence of the prototypical cholestatic drugs cyclosporine A (CsA) and chlorpromazine. Rapid inhibition of TCA clearance and recovery were found to be major characteristics of CsA. Conversely, the action of chlorpromazine was described by slow onset of inhibition relative to inhibition of TCA clearance by CsA. The established mathematical model, validated by the use of these 2 prototypical cholestatic drugs and the integration of bile canalicular dynamics, provides an important development for the further study of human hepatobiliary function, through simultaneous temporal and vectorial membrane transport of bile acids in drug-induced cholestasis.

**Key words:** human hepatocytes; HepaRG cells; mathematical model; taurocholic acid; chlorpromazine; cyclosporine A.

The underlying pathophysiological mechanisms for most hepatocellular forms of drug-induced hepatic injury remain poorly understood. However, there is reasonable evidence that intrahepatic cholestatic forms of drug-induced liver damage frequently result from a drug- or metabolite-mediated inhibition of hepatobiliary transporter systems (Goldring *et al.*, 2017; Hillgren *et al.*, 2013). In addition to the function of these key transporters in determining hepatic drug exposure and clearance, the coordinated action of these transport systems is essential for bile formation and the biliary secretion of cholephilic compounds and drugs (Chiang, 2009). A drug-mediated functional disturbance of these processes, directly or indirectly, can lead to the arrest of bile

formation and flow with the development of cholestatic liver cell damage (Pauli-Magnus and Meier, 2006). In addition to drug-mediated inhibition of hepatocellular transport function, the interindividual variability of transporter expression and function are altered by pre-existing hepatic diseases and genetic factors, which are believed to contribute to the development of drug-induced risk of cholestasis in susceptible individuals (Trauner *et al.*, 1998). Recently, some of us reported that cholestatic drugs caused alteration of bile canaliculi dynamics associated with impairment of the Rho-kinase/myosin light chain kinase signaling pathway using human HepaRG cells (Burbank *et al.*, 2016; Sharanek *et al.*, 2016).

Although the use of primary human hepatocytes (PHHs) for the study of drug effects on bile formation and secretion by hepatocytes is well documented (Guo *et al.*, 2016; Swift *et al.*, 2010), the donor-donor variability and inherent dedifferentiation of the hepatocellular phenotype in culture can often greatly influence their practical routine use in early screening in drug discovery. Moreover, these biological donor-donor variabilities associated with PHH may confound opportunities to sequentially build an integrated time-resolved mathematical model using a singularly phenotypically stable, reproducible and robust *in vitro* model by which to describe bile acid clearance and flow, and study the impact of drug effects with time in culture. By contrast, the HepaRG cell line exhibits a well-characterized and stable hepatocyte-like phenotype (Guguen-Guillouzo and Guillouzo, 2010) by which to reproducibly measure bile formation and bile canalicular (BC) clearance (Sharanek *et al.*, 2015), to establish a dynamic mathematical model describing bile acid clearance.

Modeling the flow of drugs or substrates by ordinary differential equations (ODEs) is a common approach in pharmacokinetic modeling. Indeed, mathematical models of drug disposition (Jones *et al.*, 2012; Li *et al.*, 2014) and bile flow (Guo *et al.*, 2016; Yang *et al.*, 2015) into and out of hepatocytes have been previously presented. All these models have a common model structure, including cellular, canalicular/biliary and medium compartments. Bile acids are transported between these compartments. This model structure is also used in this work. However, drug-mediated transporter inhibition is frequently modeled as a static process as the transport rates are reduced in a dose-dependent manner; time-dependence of the inhibitory process and the recovery is neglected, and the effects are assumed to occur immediately. In contrast, our model incorporates transporter inhibition as a dynamic time-resolved process into the ODE model. Also, the compartment size, such as the volume of BC that changes dynamically with the concentration of cholestatic drugs and are importantly implemented into our ODEs. These features are key events identified in the acute phase of cholestasis associated with vectorial transport of bile acids and bile flow.

In this study, we describe the use of experimental data derived from human HepaRG cells to establish a quantitative and predictive dynamic model of bile acid clearance, using a prototypical bile acid, taurocholic acid (TCA), for the study of hepatobiliary transport. A validation of the model was further achieved by use of 2 prototypical cholestatic drugs, cyclosporine A (CsA) and chlorpromazine (CPZ), previously shown to exhibit differences in the mechanisms of apical and basolateral transporter inhibition (Antherieu *et al.*, 2013; Sharanek *et al.*, 2014) and their effect on BC dynamics (Burbank *et al.*, 2016).

## MATERIALS AND METHODS

**Data sources and statistical analysis.** Chemical reagents, details of biological experiments and techniques used to prepare and characterize HepaRG cells and PHH are provided in the Supplementary Material (Section 1). In brief, wet-bench assay data from experiments with CPZ (Bachour-El Azzi *et al.*, 2014) and CsA (Sharanek *et al.*, 2014) were used to develop a mathematical model. In addition, new experiments with the use of CPZ and CsA were performed during the course of the present study with model-informed study design. At least 4

independent experiments with HepaRG cells and PHH were performed and analyzed.

**Preprocessing of time-resolved data.** For each protocol, experiments were repeated at least 4 times. Since TCA is radiolabeled, the count data follows a Poisson distribution. In our case the number of counts is in the order of  $10^2$ – $10^3$ . “For statistical analysis, it is beneficial to have normally distributed data with equal expected variance of all data points. The transformation  $n = 2\sqrt{N}$  translates the Poisson-distributed number of counts  $N$  into (almost) normally distributed numbers  $n$  with unit variance”. Differences between independent experiments,  $j$ , that exceed the expected variance are due to heterogeneity between the preparations of cultures of HepaRG cells. These differences can be attributed to a different number of cells between experiments, represented by a scaling factor  $S$ , which translates into a factors  $= 2\sqrt{S}$  of the numbers  $n$ . In total, the mathematical model to describe all replicate readouts is described;

$$n_{j,k,r}(t) = s_j \cdot n_k(t) + \epsilon_{j,k,r}(t) + \eta_{j,k,r}(t) \quad (1)$$

where  $n_{j,k,r}(t)$  is the transformed number of counts of experiment  $j$ , set-up/treatment  $k$  and replicate  $r$  at time point  $t$ . The numbers  $\epsilon_{j,k,r}(t) \sim N(0, 1)$  and  $\eta_{j,k,r}(t) \sim N(0, \sigma_{\text{celltype}}^2)$  describe random contributions due to the stochasticity of radioactive decays and heterogeneity between HepaRG cell and treatment preparations. The parameters of interest,  $n_k(t)$ , represent the true transformed number of counts for each set-up/treatment  $k$  as being used for dynamic modeling. They are determined jointly with the scaling parameters  $s_j$  and the cell-type heterogeneity  $\sigma_{\text{celltype}}$  by least-squares estimation. Parameter uncertainties  $\sigma_{n_k(t)}$  are obtained from the least-squares fit. They account for the number of replicates, the uncertainty of the estimated scaling parameters and the heterogeneity between experiments. The heterogeneity parameters  $\sigma_{\text{celltype}}$  are employed to quantify the reproducibility of experiments for the cell types HepaRG, human hepatocytes in sandwich culture and human hepatocytes in conventional culture. See Supplementary Figure 2 (Data preprocessing) for a comparison of the different cell types.

**A dynamic model of TCA transport.** TCA transport is modeled by ODEs. The equations are based on mass-action or Michaelis-Menten kinetics and account for the transport between 3 compartments, ie, incubation medium, cells (cyto) and canaliculi with volumes  $V_{\text{buffer}}$ ,  $V_{\text{cyto}}$ , and  $V_{\text{cana}}$ . A schematic overview of the model is shown in Figure 1. The basic transport processes are



where  $k_1, \dots, k_4$  denote transport rates. These rates are susceptible to temperature, calcium/magnesium and sodium changes and depend on the activity of the corresponding basolateral and canalicular membranes to TCA transport. In this study, each transport process can be associated to 1 membrane transporter known to be associated with the basolateral, sinusoidal and canalicular cell membranes, i.e. uptake ( $T_1$ ), sinusoidal efflux ( $T_2$ ) and canalicular efflux ( $T_3$ ). In summary, the rate constants are expressed by the equations

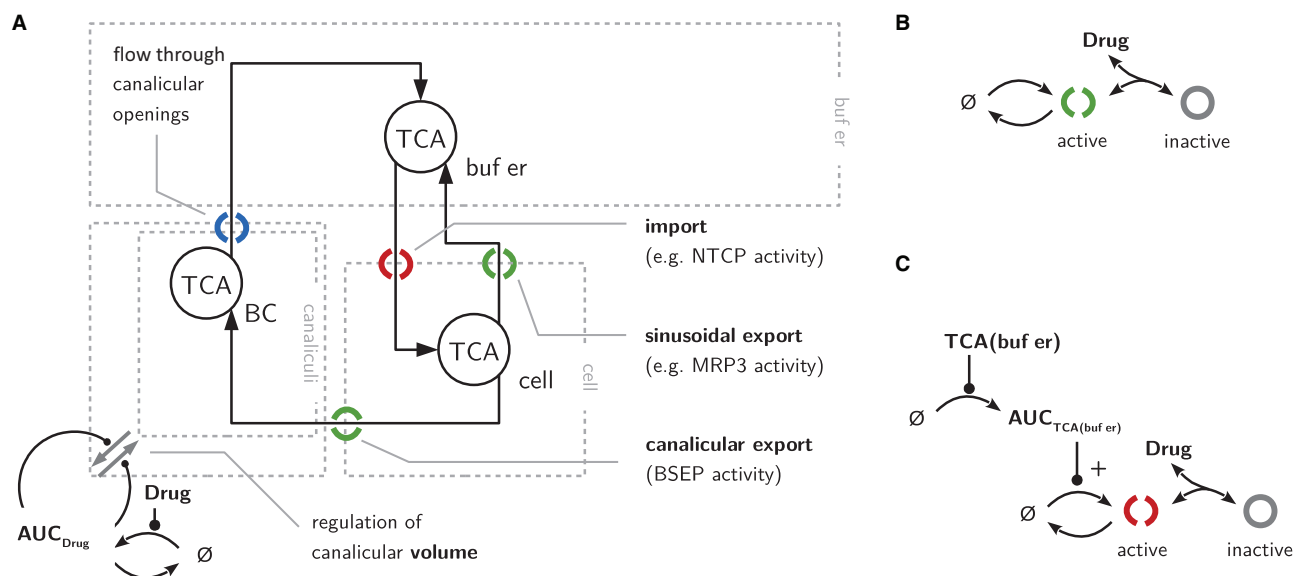


**Figure 1.** Schematic representation of the dynamic model. A, The flow of TCA between the three compartments is indicated by arrows. Transporters associated to each transport route are marked by red (uptake) and green (efflux) circular symbols. Canaliculi content ejection back into buffer is marked by a blue circular symbol. The amount of TCA in each compartment and the canaliculi volume are dynamic states. Canaliculi volume changes are induced by drug exposure. B, Drug-induced transporter inhibition is expressed by a phenomenological model which can be represented by a reaction network. During the absence of the drug, levels of the active transporter (green open circle) are in equilibrium. Upon drug stimulation, a new equilibrium between active and inactive (grey circle) transporter. C, TCA import is inhibited by the cholestatic drug. This is illustrated by the equilibrium reaction between active (red open circle) and inactive (grey circle) transporter. Additionally, continuous exposure to TCA in the buffer eventually leads to increased uptake. The regulation of active transporter is linked to the integrated buffer TCA concentration in the model. See “Materials and Methods” Section for full description. Color versions of illustrations are available in the online version.

$$\begin{aligned}
 k_1 &= \frac{k'_1 \cdot [T_1] \cdot (1 + a_1 \cdot [Na^+])}{\left(1 + d_1 \left(1 - \frac{\Delta\vartheta}{33^\circ C}\right)\right)} \\
 k_2 &= \frac{k'_2 \cdot [T_2]}{\left(1 + d_2 \left(1 - \frac{\Delta\vartheta}{33^\circ C}\right)\right)} \\
 k_3 &= \frac{k'_3 \cdot [T_3]}{\left(1 + d_3 \left(1 - \frac{\Delta\vartheta}{33^\circ C}\right)\right)} \\
 k_4 &= \frac{k'_4}{\left(1 + d_4 \left(1 - \frac{\Delta\vartheta}{33^\circ C}\right)\right) \cdot (K_4 + [Ca^{2+}])}
 \end{aligned} \quad (3)$$

where  $k'_1, \dots, k'_4$  are the transport parameters,  $\Delta\vartheta$  is the temperature change with respect to  $4^\circ C$ ,  $d_1, \dots, d_4$  denote deceleration parameters associated to a temperature drop,  $a_1$  is the acceleration parameter associated to sodium in the buffer and  $K_4$  represents the effect of calcium on canalicular efflux.

The kinetic principles used to model uptake, sinusoidal efflux and canalicular efflux is Michaelis-Menten Kinetics whereas the transport from the canaliculi compartment to the buffer compartment is modeled by mass-action kinetics.

$$\begin{aligned}
 \frac{d}{dt} TCA_{\text{buffer}} &= -\frac{k_1 \cdot TCA_{\text{buffer}}}{1 + \frac{TCA_{\text{buffer}}}{K_{\text{import}}}} + \frac{k_2 \cdot TCA_{\text{cyto}}}{1 + \frac{TCA_{\text{cyto}}}{K_{\text{baso}}}} + k_4 \cdot TCA_{\text{cana}} \\
 \frac{d}{dt} TCA_{\text{cyto}} &= \frac{k_1 \cdot TCA_{\text{buffer}}}{1 + \frac{TCA_{\text{buffer}}}{K_{\text{import}}}} - \frac{k_2 \cdot TCA_{\text{cyto}}}{1 + \frac{TCA_{\text{cyto}}}{K_{\text{baso}}}} - \frac{k_3 \cdot TCA_{\text{cyto}}}{1 + \frac{TCA_{\text{cyto}}}{K_{\text{cana}}}} \\
 \frac{d}{dt} TCA_{\text{cana}} &= \frac{k_3 \cdot TCA_{\text{cyto}}}{1 + \frac{TCA_{\text{cyto}}}{K_{\text{cana}}}} - k_4 \cdot TCA_{\text{cana}}
 \end{aligned} \quad (4)$$

The transporter activity  $T_i$ ,  $i = 1, \dots, 3$ , is dynamically regulated being modeled by the reactions  $\emptyset \xrightarrow{\alpha_i} T_i$ . Where, “ $\rightarrow \emptyset$ ” and “ $\emptyset \rightarrow$ ” denote deregulation and production. The parameterization by  $\alpha_i$  implies that the equilibrium of the reaction is  $T_i = 1$  for all transporters and the time-scale how quickly the disturbed system returns to the initial measures of TCA clearance is determined by the value of  $\alpha_i$ . TCA clearance in control incubations can in the meantime be reduced by cholestatic drugs. Within the mass-action formalism, inhibition by a drug is implemented as



where  $D$  is the drug and  $DT_1, \dots, DT_3$  are the inhibited transporters, see Figure 1B. The rate parameters  $k_{+}^{(i)}$  represent the effective inhibition of the drug on transporter  $T_i$  while  $k_{-}^{(i)}$  represents the transporters' ability to recover when the compound-containing buffer is removed.

In the absence of the drug, membrane-associated transport activity is equal to unity and assigned the value of 1 across the membranes. By the addition of the drug, a new equilibrium between active and inactive membrane transport activity is approached which is determined by the equilibrium constants  $K_c^{(i)} = \frac{k_{+}^{(i)}}{k_{-}^{(i)}}$ . Conversely, when the free drug is removed, the system transitions to another equilibrium retaining some of the drug's inhibitory effect for reversible inhibition of transporter activity. The drug-induced dynamics is overlain by the transporter regulating mechanism steering all transporter activities associated to membranes to unity of 1. The possibility of irreversible changes of the transporter activity is equally incorporated into the model by

choosing drug-specific values for the membrane transporter activity,  $\alpha_i$ .

When cells are exposed to TCA for more than 30 min, the uptake can be seen to effectively accelerate. This is possibly accounted for by changes in membrane transport with time of TCA exposure in culture. In our model, TCA uptake is controlled by the  $T_1$  state variable. To account for the accelerated uptake, we include a gain term for the  $T_1$  state, proportional to the integrated TCA buffer concentration, area under the curve  $(AUC)_{TCA(buffer)}$ , see Figure 1C. In summary, the transporter dynamics is described by the differential equations.

$$\begin{aligned} \frac{d}{dt}T_1 &= \alpha_1 \cdot (1 - T_1) - k_+^{(1)} \cdot D \cdot T_1 + k_-^{(1)} \cdot DT_1 + b \cdot AUC_{TCA(buffer)} \\ \frac{d}{dt}T_2 &= \alpha_2 \cdot (1 - T_2) - k_+^{(2)} \cdot D \cdot T_2 + k_-^{(2)} \cdot DT_2 \\ \frac{d}{dt}T_3 &= \alpha_3 \cdot (1 - T_3) - k_+^{(3)} \cdot D \cdot T_3 + k_-^{(3)} \cdot DT_3 \\ \frac{d}{dt}AUC_{TCA(buffer)} &= TCA_{buffer} \end{aligned} \quad (6)$$

Besides their effects on membrane transporter activity, cholestatic drugs can have both constriction and dilatation effects on BC, such that the volume of the canalicular compartment is either reduced or increased. For low CsA concentration treatments, the dilatation effect prevails whereas for higher doses constriction of BC are observed. This behavior can be implemented by a linear and a saturating rate for dilatation and constriction:

$$\emptyset \xrightleftharpoons[k_-]{k_+} AUC_{Drug}, \quad V_{BC} \xrightleftharpoons[k_{build} + AUC_{Drug}]{AUC_{Drug}} \emptyset \quad (7)$$

The dilatation/constriction rates are linked to the integrated drug concentration over time, see Figure 1A. The integrated drug concentration is restricted by a reduction of the rate,  $k_-$ . Because we expect a certain delay between drug treatment and reduction of the volume, canalicular volume constriction is linked to the integrated drug concentration  $AUC_{drug}$  instead of simply drug concentration.

A list of all reactions and the corresponding differential equations are available in the Supplementary Material Section 3 (Model Specification).

**Parameter estimation and uncertainty analysis.** Parameter estimation is based on the maximum-likelihood method. As discussed in the section on preprocessing of time-resolved data, the observational noise is composed of a random contribution due to the stochasticity of radioactive decays and a random contribution due to the heterogeneity between repeated preparations. Although results for the HepaRG cell line are highly reproducible, heterogeneity  $\sigma_{celltype}$  still presents the major contribution to the observation noise of around 15%.

Maximization of the likelihood is equivalent to minimization of the objective function

$$\chi^2(p) = \sum_{ij} \frac{(x_j(t_i, p) - x_{j,i}^D)^2}{\sigma_{ij}^2} \quad (8)$$

where  $x_j(t_i, p)$  denotes the model prediction for state  $j$  at time-point  $t_i$  given the parameter values  $p$ . The squared residuals between model prediction and data points  $x_{j,i}^D = \frac{n_j^D(t_i)}{4}$  are weighted

by the variances  $\sigma_{ij}^2 = \frac{n_j^D(t_i)}{4} \sigma_{celltype}^2$ . Optimization of the objective function is performed by a trust-region algorithm (Nocedal and Wright, 2006) that relies on derivative information. Therefore, the ODEs of the dynamic system are combined with their forward sensitivity equations (Leis and Kramer, 1988) and solved numerically by the LSODES integrator (Soetaert et al., 2010). Nonlinear optimization is usually compromised by the existence of several local optima. To search the parameter space for the best optimum, we follow a multi-start strategy to initialize the trust-region optimizer. Identification of the parameter determinants has been checked based on the symmetries that are admitted by the system (Merkt et al., 2015). Practical non-identifiability and parameter confidence bounds were analyzed using the profile likelihood method (Kreutz et al., 2013; Raue et al., 2009).

All analyses have been performed in R with the packages cOde/dMod (Kaschek et al., 2016) for dynamic modeling and parameter estimation in R, available on Comprehensive R Archive Network. More details about the parameter estimation process are available in the Supplementary Material Section 4 (Model Fitting and Model Reduction).

## RESULTS

The results described in this work are based on dynamic modeling in combination with parameter estimation to match the experimental TCA data with our mathematical model. Thus, the nature of our model turns from being descriptive to being predictive. The model of TCA transport in HepaRG cells is based on ODEs describing the TCA flux between three compartments; incubation medium, cells and canaliculi. The impact of the cholestatic drugs CsA and CPZ on uptake and efflux activities has been implemented as a dynamic process with changing transporter activity and canalicular volume over time.

The experimental conditions are characterized by different treatments times, incubations times or changing  $Ca^{2+}/Mg^{2+}$  levels in the buffer. These conditions are fully accounted for by the model which ultimately depends on a single set of parameters. From these parameter values, the simulated model outcome is uniquely determined for all experimental conditions. The building of the model was achieved by use of 4 different experimental protocols, 2 efflux and 2 uptake protocols. For the sake of clarity, these protocols with the corresponding model predictions are discussed separately, keeping in mind that they are connected by a single model structure and parameter set.

### Temperature and $Ca^{2+}/Mg^{2+}$ Conditions

The first protocol sheds light on the temperature dependency of transport rates and shows how strongly the presence of  $Ca^{2+}/Mg^{2+}$  in the buffer contributes to the formation of canalicular junctions to retain TCA in the canaliculi. Figure 2 shows the efflux dynamics of [ $^3$ H]-TCA in the cells and in the buffer at 2 temperature conditions, 37 °C and 4 °C, and 2 buffer conditions, with and without  $Ca^{2+}/Mg^{2+}$ . Cellular levels of [ $^3$ H]-TCA (Figure 2A), remain almost constant for low temperature (blue) while showing a quick reduction at 37 °C (red).

In building the dynamic model of TCA transport, we introduced deceleration parameters  $d_1, \dots, d_4$  to express the change of transport rates from 37 °C to 4 °C. Exploring the parameter space, we found several locally optimal solutions that explained the temperature and  $Ca^{2+}/Mg^{2+}$  dependency as shown in Figure 2A. Locally optimal solutions involved either dominant deceleration of sinusoidal/canalicular efflux mediated TCA transport or dominant deceleration of canalicular efflux.

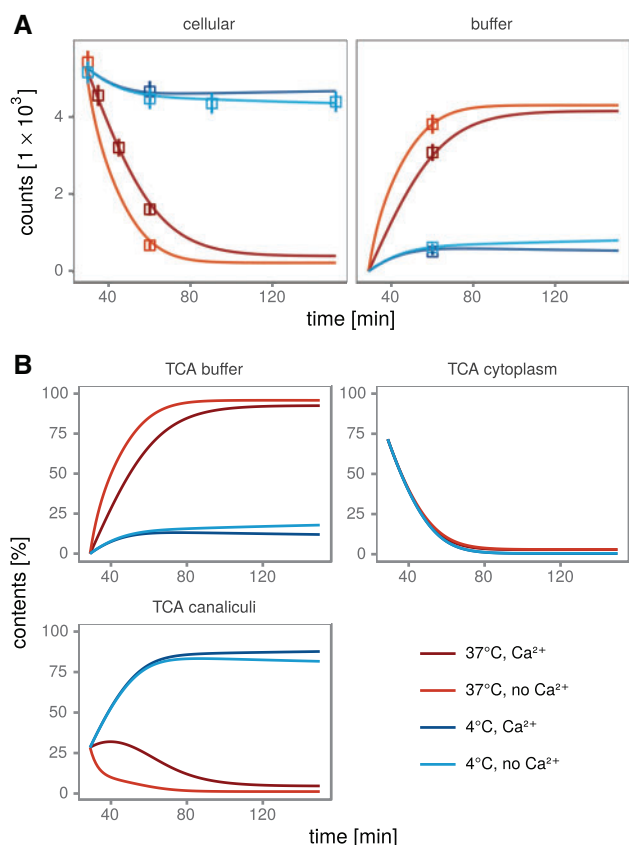


**Figure 2.** TCA efflux in HepaRG cells. Cells incubated at either 37 °C or 4 °C during efflux and the efflux buffer did or did not contain calcium (colors). A, Data points and model fit are shown as dots and lines, respectively. B, The model prediction for the distribution of TCA amounts between the three compartments shows canalicular levels after uptake to be around 25%. Color versions of illustrations are available in the online version.

However, only the latter solution is able to reproduce the pronounced effect between  $Ca^{2+}/Mg^{2+}$  and  $Ca^{2+}/Mg^{2+}$ -free conditions at 37 °C while, at the same time, showing no difference at 4 °C.

The dynamic model allows separation of the intracellular and canalicular contributions which summarized, represents the observation of cellular TCA content. Together with a priori knowledge about the total TCA amounts, a prediction of the  $[^3H]$ -TCA distribution throughout the compartments is feasible, shown in Figure 2B. After 30 min uptake, 75% of all TCA is located in the cytoplasm of cells and 25% in the canaliculi. Under calcium-free conditions at 37 °C, it takes around 10 to 20 min for the canalicular junctions to disrupt, as can be seen from the model prediction for canalicular TCA.

#### Efflux of TCA in the Presence of Cholestatic Drugs

The second protocol focuses on the inhibitory effect of the cholestatic drugs CsA and CPZ on TCA efflux. HepaRG cells were incubated with  $[^3H]$ -TCA for 30 min and then treated for 2 h in the presence or absence of drug in standard buffer containing  $Ca^{2+}/Mg^{2+}$ . The experimental results and corresponding model fits are shown in Figure 3. Cellular levels of TCA over a time period of 120 min are shown in Figure 3A. With increasing concentrations, CsA-treated cells (squares and solid lines) show the expected inhibition of TCA efflux. To obtain a measurement that reflects the cytoplasmic TCA level as close as possible, the

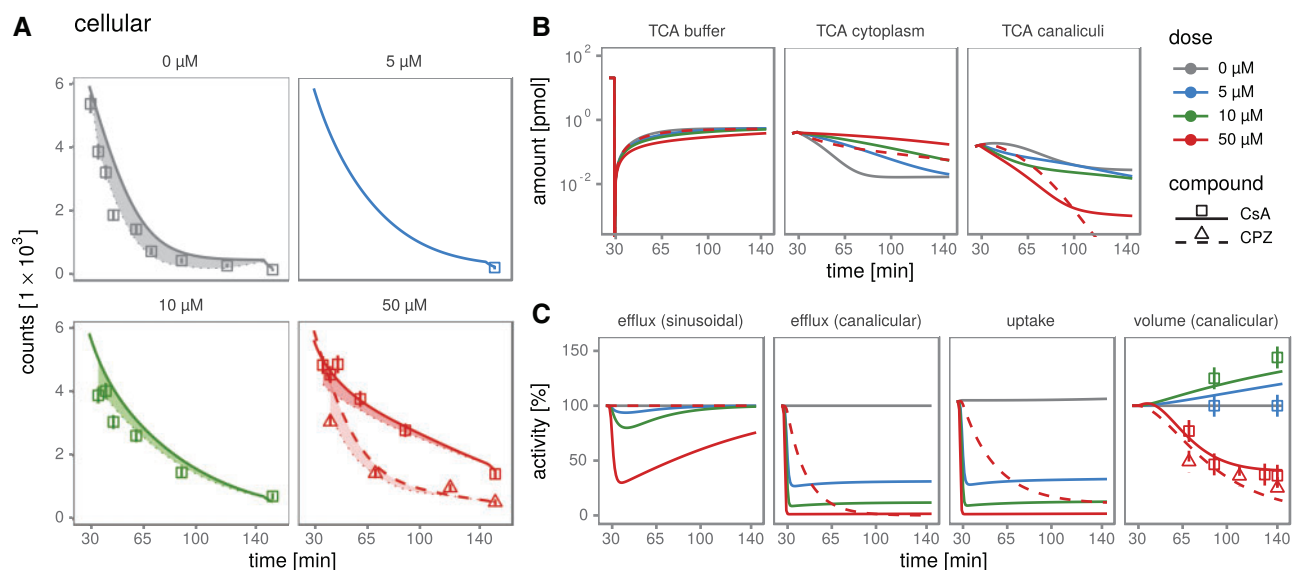
efflux buffer was exchanged by a  $Ca^{2+}/Mg^{2+}$ -free medium is added after incubation with  $[^3H]$ -TCA and drug to measure total TCA efflux. The buffer exchange has been included as a discontinuity into the mathematical model. Therefore, for each data point there is 1 corresponding model trajectory to fit this data points. The typical trajectory shows a slow exponential decay followed by a fast transition caused by the disruption of canalicular junctions before returning to a slow decay. The range in which the cytoplasmic TCA contents changes due to the buffer exchange is shown as shaded area. The bottom part of the shaded area, a dotted line, reflects the TCA concentration after buffer exchange which is to be compared with the data points. Relative to CPZ, CsA shows a much stronger inhibitory effect on TCA clearance by comparison with CPZ at a dose of 50  $\mu$ M.

Figure 3B shows the predicted absolute amounts of TCA in the different compartments for an efflux buffer with  $Ca^{2+}/Mg^{2+}$ . All active transport processes are inhibited by CsA, as shown by Figure 3C and remain low over 120 min except for multidrug resistance-associated protein 3 (MRP3) as confirmed by immunostaining (Sharaneek *et al.*, 2015), which begins to recover cellular efflux of TCA over the period following addition of CsA. CPZ has no apparent inhibitory effect on sinusoidal efflux, albeit in the model is shown to inhibit uptake and canalicular efflux. The most evident difference between CsA and CPZ is the slower time scale by which CPZ inhibits uptake and canalicular efflux. Therefore, cells treated with 50  $\mu$ M of CPZ are able to clear almost all of the contained TCA although canalicular efflux transporters activity drops to almost 0% as similarly observed for CsA.

The inhibitory constant ( $K_i$ ) reflects binding affinity and functional strength for the inhibition of activity and becomes important for helping to predict clinically relevant drug interactions. These are normally reported as static measures. Figure 3C indicates that transporter recovery and different time scales of CsA and CPZ action are major characteristics of the system. These properties being identified by our semi-mechanistic drug-transporter response cannot be captured by a classical inhibition model ie, based on  $K_i$  values, as shown in the Supplementary Material. Exposure to high concentrations (50  $\mu$ M) of either cholestatic drug resulted in constriction of BC as early as 2 h (Figure 3C, canalicular volume). At lower concentrations (5–10  $\mu$ M), only CsA exhibited an effect characterized by bile canaliculi dilatation as shown by phase-contrast microscopy in Figure 4.

#### Uptake of TCA in the Presence of Cholestatic Drugs

The third protocol was performed to investigate the effect of treatment time on the concentration-dependent inhibitory effect of CsA. The results are shown in Figure 5. The effects of the CsA on BA uptake was estimated through measurement of intracellular accumulation of  $[^3H]$ -TCA. Briefly HepaRG cells were treated for 15, 30, or 60 min with different concentrations of CsA (0, 1, 5, 10, 25, and 50  $\mu$ M) and measurements were taken 10 min after incubation with TCA. CsA induced a dose-dependent inhibition of TCA uptake as early as 10 min after treatment. On the other hand, TCA levels of equivalent doses for different treatment times roughly achieve the same response (see Figure 5A). This is also reflected in the predicted absolute amounts in the three compartments (Figure 5B). In accordance with the observation, the estimated time-scale parameters for transporter inhibition are fast enough to realize the full inhibitory effect within few minutes (Figure 5C). During incubation with  $[^3H]$ -TCA, no drug is contained in the incubation buffer. The membrane transporter activity can recover and regain their activity to some extent during this phase. The curves for canalicular export and uptake transporter activity are almost exactly



**Figure 3.** TCA efflux in HepaRG cells in the presence of cholestatic drugs. Transporters have been inhibited by different concentrations (colors) of the cholestatic drugs CsA (0, 5, 10, and 50  $\mu\text{M}$ ) and CPZ (50  $\mu\text{M}$ ) marked as linestyles and symbols. The buffer was exchanged by a calcium-free buffer 5 min before taking the measurement. **A**, Measured cellular TCA (counts are  $\text{dpm} \times 10^3$ ). Data points and model prediction are shown as dots and lines. At low doses, canalicular efflux due to calcium removal reduces the observed cellular TCA levels significantly. **B**, The model predicts 1% uptake of all TCA in the buffer. Amounts are in pmol Avogadro. **C**, Transporter inhibition and volume constriction as predicted by the mathematical model shows a slower dynamics of CPZ-induced inhibition compared with CsA and significant volume constriction of BC only at higher concentrations. Color versions of illustrations are available in the online version.

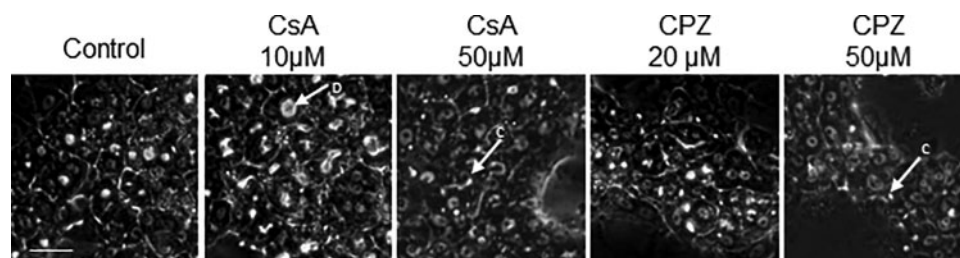


**Figure 4.** Alteration of BC morphology by CsA and CPZ in HepaRG cells. Untreated cells and cells treated with CsA (10 and 50  $\mu\text{M}$ ) or with CPZ (20 and 50  $\mu\text{M}$ ). Phase-contrast images were captured after 2 h (bar = 30  $\mu\text{m}$ ); White arrows indicate BC constriction (CsA 50  $\mu\text{M}$ ; CPZ 50  $\mu\text{M}$ ) and dilatation (CsA 10  $\mu\text{M}$ ).

superimposable, producing the same efflux dynamics whether the treatment with CsA was for 15, 30, or 60 min. By parameter estimation we find that TCA transport to the canaliculi is 4 times higher than sinusoidal export, limiting the possible impact of sinusoidal export on the shape of the curves. This relative preferential clearance of TCA is confirmed by the observed activities of bile salt transport pump (BSEP) and MRP3 activities in heterologous expressed vesicle membranes (unpublished observations). Similarly since we observe cellular uptake of TCA, the reduction of canalicular volume has no direct feedback on the observed cellular levels.

Finally, by the fourth experimental protocol, the effects of the 2 cholestatic drugs, CPZ and CsA, on bile acids uptake was estimated through measurement of intracellular accumulation of [ $^3\text{H}$ ]-TCA. HepaRG cells were treated for 30 min with either drug and then loaded with [ $^3\text{H}$ ]-TCA for different time points over 120 min. As shown in Figure 6 our model predicts that the TCA dynamics upon CPZ treatment is more linear than upon CsA treatment and turns earlier into the phase of accelerated uptake (Figure 6A). This is also visible in the predicted intracellular TCA levels, (Figure 6B) which show a different shape for CsA and CPZ. Although the exposure to high TCA concentrations for more than 2 h might be nonphysiological, the insight that continuous TCA exposure could lead to

increased TCA uptake is valuable for future mathematical model development.

Evaluating the ratio between intracellular and canalicular TCA amounts by the mathematical model, we find 2–4 times more TCA intracellular content than in the canaliculi. The ratio is even higher for higher drug concentrations. All these observations are in line with the estimated effects of CsA and CPZ on the transporter activity shown in Figure 6C. CPZ inhibition is slower, but more sustained and its effect on canalicular export and cellular uptake is similar. Also, CsA inhibition of basolateral uptake is similar to efflux inhibition. The effect is more immediate for CsA than for CPZ but transporters can partially recover after the removal of CsA. The strongly inhibited accumulation of TCA in the cells upon CsA treatment is supported by the quick recovery and over compensation of sinusoidal response, which can be attributed to sinusoidal transporter activity.

#### Primary Human Hepatocytes

We relate our findings on HepaRG cells to the TCA efflux dynamics observed in human hepatocytes. Hepatocytes were kept in either conventional (CCHH) or sandwich (SCHH) cultured human hepatocytes. The direct comparison of cellular TCA levels is shown in Figure 7.

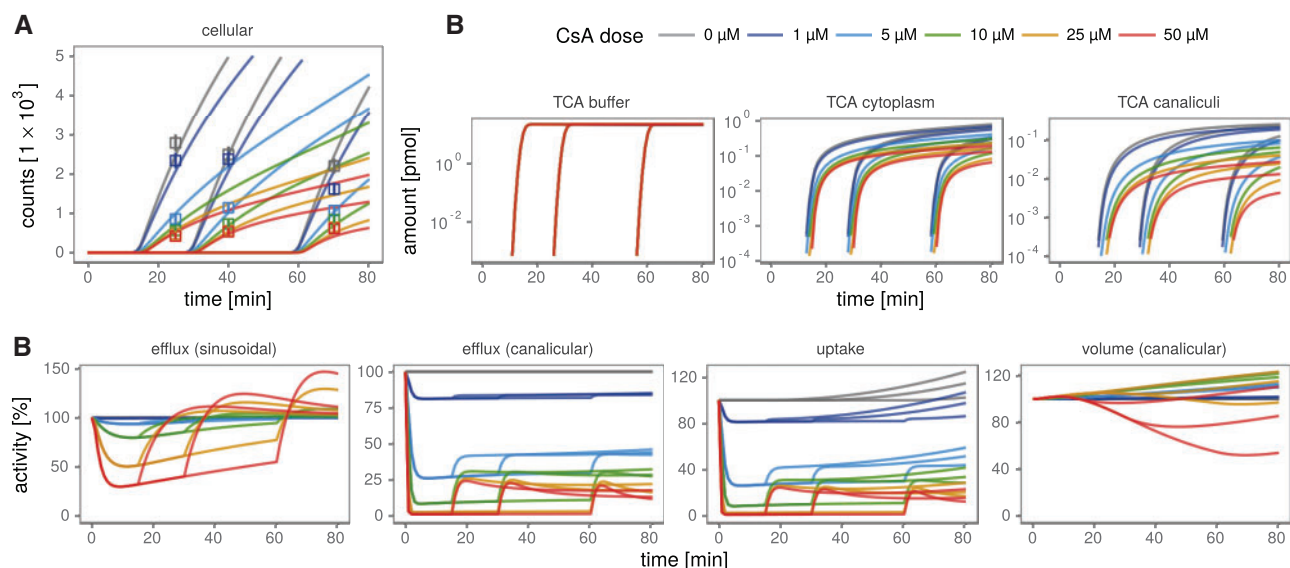


**Figure 5.** TCA uptake in HepaRG cells at different CsA treatment times. A, HepaRG treated with 0–50  $\mu\text{M}$  CsA for 15, 30 or 60 min, then change of buffer containing  $\text{H}^3$ -TCA for 10 min prior to measurements of CA. Cells have been treated with different doses (colors) of CsA for 15, 30 or 60 min and then incubated by TCA for 10 min. B, The model predicts similar TCA uptake dynamics in absolute amounts, independent of the treatment time. C, The efflux across sinusoidal, canalicular membrane and uptake are similarly predicted irrespective of time of treatment at 0–50  $\mu\text{M}$  CsA are described. Replacing the treatment-buffer with the TCA-incubation buffer, results in partial recovery of transporter inhibition (the transporter inhibition is partially reduced). Color versions of illustrations are available in the online version.

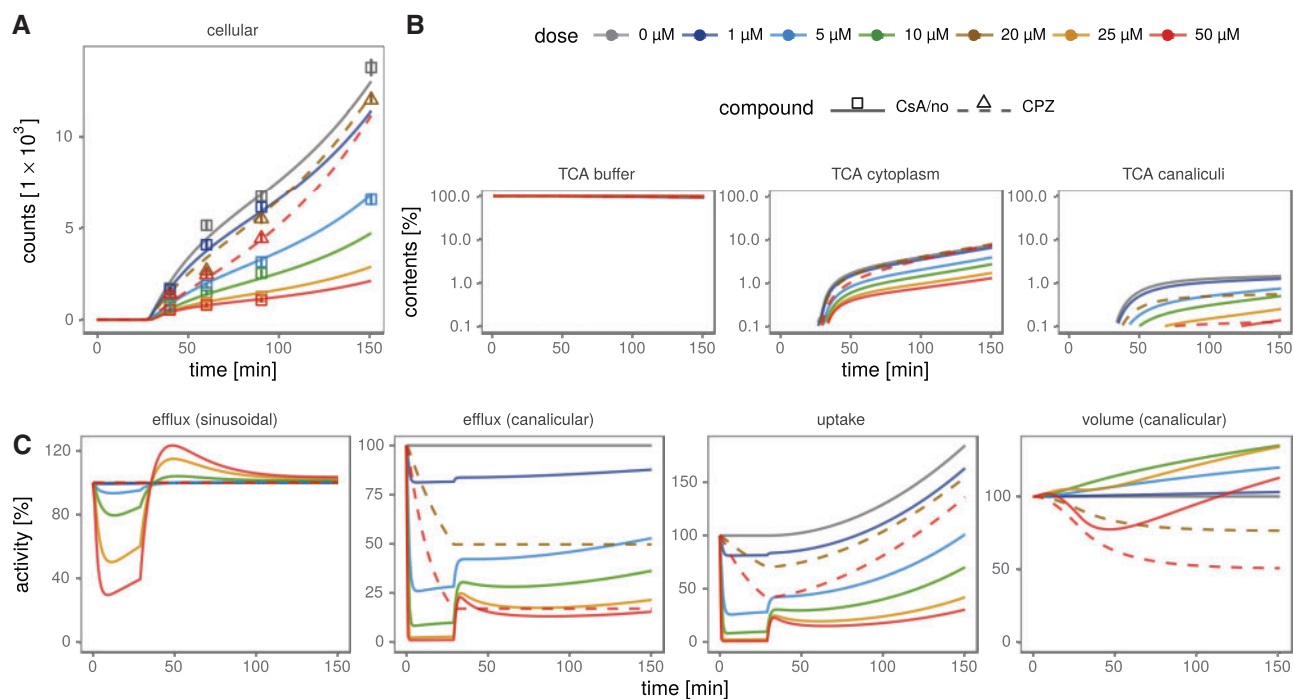


**Figure 6.** TCA uptake in HepaRG cells for different TCA incubation times. After a fixed treatment time of 30 min, either with CsA or CPZ (line-type and symbols), the cells have been incubated with TCA for different times up to 120 min. A, The data show an accelerated uptake of TCA at later time points. B, Canalicular TCA amounts, expressed as percentages, are predicted to be smaller than cytoplasmic amounts by a factor of 2–4, which is even reinforced by the cholestatic drugs. C, Uptake and canalicular export transporters show almost irreversible predicted inhibition, especially for CPZ. Uptake is increased due to the continuous exposure to TCA in the buffer. Color versions of illustrations are available in the online version.

The measurements in HepaRG cells, CCHH and SCHH are normalized by the respective mean values at  $t = 30$  min, just before the uptake buffer is replaced to measure efflux. Since the efflux is approximately described by an exponential curve, differences between the cell types are visualized on the log-scale where a steeper slope corresponds to a higher export rate.

On average, the human hepatocytes show a faster export of TCA. The efflux from human hepatocytes is not stopped at  $4^\circ\text{C}$  but is in the same range as at  $37^\circ\text{C}$  with  $\text{Ca}^{2+}/\text{Mg}^{2+}$  in the buffer; conventional cultured hepatocytes are partly affected. There is the tendency that human hepatocytes are more susceptible to  $\text{Ca}^{2+}/\text{Mg}^{2+}$  removal which might indicate that BC tight junctions

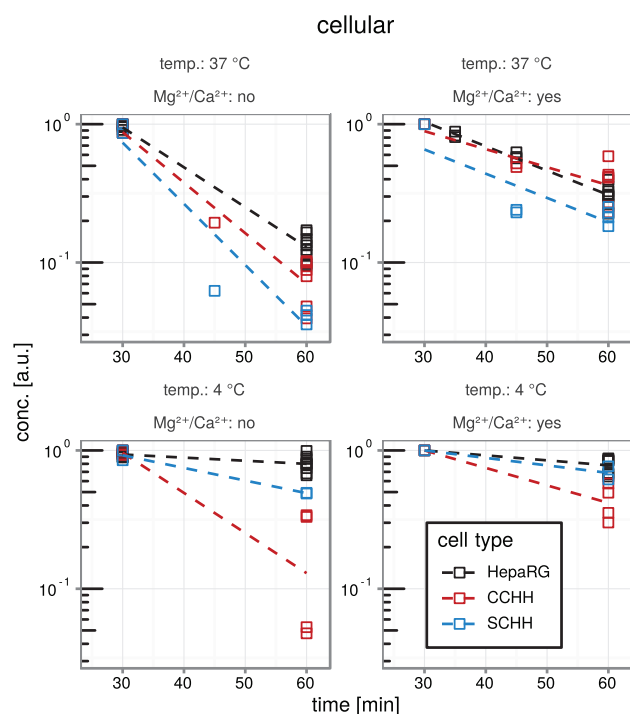


**Figure 7.** Comparison of TCA efflux in HepaRG cells and human hepatocytes for different temperature and  $\text{Ca}^{2+}/\text{Mg}^{2+}$  conditions. Radioactive counts were normalized by time point 30 min. The normalized counts reflect cellular TCA concentrations, shown by squares, on a logarithmic scale. Colors indicate the cell type. Differences between the cell types are highlighted by dashed lines which are computed by linear regression from the data points. Although on average human hepatocytes show greater efflux activity than HepaRG cells, the efflux rate under standard conditions ( $37^\circ\text{C}$  and  $\text{Ca}^{2+}/\text{Mg}^{2+}$ ) remains broadly unaffected, as indicated by the similar slope of all three regression lines. Color versions of illustrations are available in the online version.

are perhaps more disposed to  $\text{Ca}^{2+}$  depletion, which in CsA-treated PHH is supported by the observation of fewer fully closed BC in culture.

The comparative analysis of all data reveals that the variability in CCHH and SCHH is much larger than in HepaRG cells see Section 2 Data-Preprocessing in the Supplementary Material. This was to be expected due to the known donor-donor differences in transport activity and intracellular amounts of bile acids. This is attributable at least in part due to source of resection tissue from patients, the hepatocytes of which may carry some functional and phenotypic changes related to the donor. These changes may not necessarily be associated with normal healthy liver tissue, thus corroborating our approach to start with a mathematical model of HepaRG cells by which to study the simultaneous effect of TCA transport, BC volume and drug effect. Despite the observed donor-donor differences with PHH, it is nevertheless feasible future work using the model established with HepaRG cells can potentially form the basis of further studies using PHHs. This opens the perspective of pointing towards extending our work with the use of PHHs for the development of models to eventually incorporate donor-donor differences, using the dynamic mathematical model described herein.

## DISCUSSION

In this study, we describe a dynamic mathematical model of TCA uptake and clearance on the basis of experimental data

obtained with untreated and CsA- and CPZ-treated human HepaRG cells. Data from both previously performed and new experiments on untreated and drug-treated cells were analyzed. All our results were obtained by dynamic modeling of time-resolved experimental data and parameter estimation. Our basic model of bile acid transport was established on ODEs and was extended by a dynamic drug-effect model introducing transporter activity and canalicular volume as dynamic states. These features are important components of bile acid secretion and flow, the deregulation of which are implicated in drug-induced cholestasis (Watanabe et al., 1991, 2007).

We analyzed TCA clearance by measuring uptake and both canalicular and sinusoidal efflux that are predominantly performed by sodium-taurocholate co-transporting polypeptide (NTCP), BSEP, and MRP3 membrane transporters, respectively. Although passive diffusion is reported for some bile acids the predominant clearance of the prototypical bile acid, TCA, for hepatobiliary studies is through active transport by the involvement of these membrane transporters. In untreated cells, TCA was found in the three compartments, ie, cells (intracellularly), BC lumen and medium after a short incubation. Time-dependent increased accumulation in the medium during the 30 min incubation likely reflected an increased sinusoidal efflux associated with the activation of the MRP3 membrane transporter in the presence of drugs, which has been described as a compensatory mechanism in the event of BSEP inhibition (Yang et al., 2013). In support of this, immuno-localization of MRP3 showed a more intense labeling of the sinusoidal membrane after 30 min of CsA treatment (Sharanek et al., 2015). However, it cannot be excluded that a fraction of TCA was effluxed to the supernatant via BC. Indeed, we recently showed that BC exhibit asynchronism contraction and relaxation cycles of around 60 min each to evacuate BC content into the supernatant (Sharanek et al., 2016).

In our model, membrane transporter activity returns close to its basal level following CsA treatment. By parameter estimation we found that this regulatory mechanism could play a major role for sinusoidal export but not for cellular uptake and canalicular export. The model favors a scenario where sinusoidal transporters quickly recover after CsA treatment and restores full sinusoidal membrane transporter activity, whereas for uptake and canalicular export transporters the recovery of activity remains partially inhibited. Consequently, TCA export is shifted from canalicular to sinusoidal export which, under normal conditions, contributes only 20% to the total export. Thereby, the sinusoidal membrane transporter activity confirms its role as an alternative route of TCA exports when the canalicular membrane transporter (ie, BSEP) is inhibited. These observations hold promising insights for the study on the simultaneous inhibition and recovery of membrane transporter activities in acute drug-induced cholestasis. Further work to extend these observations to other cholestatic drugs will provide important developments to establish if the effects of CsA and CPZ on membrane transporters are drug specific, or equally applies to potent cholestatic drugs and rarely cholestatic drugs.

Inhibition of transporter activity by the 2 prototypical inhibitors, CsA and CPZ, was modeled phenomenologically by reversible and irreversible binding reactions. Parameter estimation revealed that all transporters have a well-defined forward- and backward reaction to CsA due to competitive inhibition characteristics of CsA. This means that the time-scales of inhibition and recovery as well as the extent of inhibition during and after CsA treatment can be uniquely determined from the time-course experiments for the three membrane containing

transporters. CPZ which is an inhibitor of cellular uptake and canalicular export but not sinusoidal export (Antherieu *et al.*, 2013) was found to act on TCA clearance rates more slowly when compared with CsA. In agreement, by parameter estimation we could show that inhibition by CPZ is irreversible, the 2 reaction parameters corresponding to reversibility being compatible with zero. Indeed, experimental studies showed that the cholestatic mechanism of CPZ is indirect and slower, depending on generation of reactive oxygen species that lead to irreversible bile flow inhibition (Antherieu *et al.*, 2013). This indicates that the mathematical model is capable of distinguishing between the 2 cholestatic drugs which act by different mechanisms. In addition, the effect on clearance by both CsA and CPZ causes reduction of canalicular size which was confirmed by direct light microscopic observation. Therefore, the canalicular volume was included as a dynamic state into the mathematical model. We found that the volume reduction is well described when linked to compound exposure and effect on TCA clearance. These features are important when considering testing unknown drug safety profiles for cholestasis in drug discovery. Moreover, the model predicts  $K_i$  and can be extended to the study of drug-drug interactions, bile acid perturbation and BC deregulation in drug safety testing. The assessment of  $K_i$  was performed by 2 approaches in our work with generally comparable results (Supplementary Material Section 5). The observed differences by 2 the approaches can be attributed to the temporal effect of inhibition and transport recovery. The ability to model both inhibition and recovery can provide important insight when defining drug safety by use of the dynamic model.

Finally, to validate that data from experiments on HepaRG cells are adequate to build a physiologically relevant mathematical model, we analyzed sets of data on TCA uptake and efflux from PHH. As expected, the mathematical analysis of all data reveals expected variability in PHH clearance of TCA that was considerably larger than in HepaRG cells attributed to the statistical fluctuations of inter-donor variability. By contrast, statistical analysis of HepaRG cells data showed high inter-assay reproducibility, further supporting the stable phenotype of this cell line and its suitability to construct a mathematical model to explore for the first time the hepatobiliary function and apparent inter-relationship of membrane transport, BC dynamics by drug-induced impairment of TCA clearance. Use of HepaRG cells, which confers stable biological phenotype without donor-donor phenotypic variabilities associated with isolated PHHs, would permit use in the screening and modeling of novel drug candidates in pharmaceutical drug discovery. The approach herein would equally contribute to known works on Systems Pharmacology Modeling that describe delayed bile acid mediated drug-induced hepatotoxicity by use of Physiologically based pharmacokinetics (PBPK) and virtual population approaches previously described in Yang *et al.* (2014).

Our model further identifies a number of similarities and dissimilarities between TCA clearance in HepaRG cells, CCHH and SCHH. In standard experimental conditions of temperature (37°C) and Ca<sup>2+</sup>/Mg<sup>2+</sup>-containing buffer, similar TCA efflux rates were observed and a temperature-dependent effect was also observed with the linear regression model. Indeed, the mathematical curves showed a decrease of TCA active transport in the three cell models at 4°C as indicated by the smaller slope of the regression lines. However, even though the efflux rates were close, human hepatocytes showed a tendency for a faster export of TCA than HepaRG cells that can be attributed to the known higher constitutive expression of BSEP protein at the canalicular

membrane (Bachour-El Azzi *et al.*, 2015) and a higher number of hepatocytes per surface unit in PHH cultures. The higher level of BSEP expression in PHH thus confers the capacity ( $V_{max}$ ), but not the ability ( $K_m$ ) to transport TCA across the BC membrane. The primitive biliary cell population present in HepaRG cell cultures do not exhibit any of the bile acid transporters and do not contribute to uptake and accumulate bile acids (Sharanek *et al.*, 2014). CCHH were less susceptible to low temperature and reduction of TCA efflux at 4°C and was less pronounced compared with either HepaRG cells or SCHH. Importantly, while HepaRG cells are maintained for 30 days in culture to reach differentiation, human hepatocytes are only maintained for 4–5 days before use. In this short culture period, isolated human hepatocytes in sandwich configuration recover to form tight-junctions and well-sealed BC by comparison with conventional collagen culture conditions of cells (LeCluyse *et al.*, 1994; Liu *et al.*, 1998). Similarly, as observed with HepaRG cells, the regression model revealed a dependency of BC tight junctions on Ca<sup>2+</sup>/Mg<sup>2+</sup> in human hepatocytes. It also showed that PHH are more vulnerable to cation depletion than HepaRG cells. Due to the long culture period, HepaRG cells developed tight junctions of larger size than in human hepatocytes and thus are less sensitive to a Ca<sup>2+</sup>/Mg<sup>2+</sup> depletion. It may also be possible that CCHH have more poorly formed junctions and consequently accumulate less bile acids in canalicular lumens than their SCHH counterparts and thus potentially diffusion of bile acids to possibly explain the apparent and reduced susceptibility to 4°C and higher vulnerability to cation depletion observed in this study. Nevertheless, if some differences were observed between HepaRG cells and PHH, the largely similar clearance of TCA between these 2 cell models open the perspective of future developments of refining the mathematical model described herein for use in extending this work to explore mechanisms of hepatobiliary regulation e.g. FXR gene regulation of transporters in HepaRG cells and inter-individual variabilities in the transport of bile acids and BC kinetics using phenotypically characterized PHHs.

## SUPPLEMENTARY DATA

Supplementary data are available at *Toxicological Sciences* online.

## FUNDING

This work was supported by the European Community (Contract MIP-DILI-115336). The MIP-DILI project has received support from the Innovative Medicines Initiative Joint Undertaking, resources of which are composed of financial contribution from the European Union's Seventh Framework Programme (FP7/20072013) and EFPIA companies' in kind contribution. <http://www.imi.europa.eu/>. Daniel Kaschek and Ahmad Sharanek were financially supported by the MIP-DILI project.

## REFERENCES

- Antherieu, S., Bachour-El Azzi, P., Dumont, J., Abdel-Razzak, Z., Guguen-Guillouzo, C., Fromenty, B., Robin, M. A., and Guillouzo, A. (2013). Oxidative stress plays a major role in chlorpromazine-induced cholestasis in human HepaRG cells. *Hepatology* 57, 1518–1529.
- Bachour-El Azzi, P., Sharanek, A., Abdel-Razzak, Z., Antherieu, S., Al-Attrache, H., Savary, C. C., Lepage, S., Morel, I., Labbe, G., Guguen-Guillouzo, C., *et al.* (2014). Impact of inflammation

- on chlorpromazine-induced cytotoxicity and cholestatic features in HepaRG cells. *Drug Metab. Dispos.* **42**, 1556–1566.
- Bachour-El Azzi, P., Sharanek, A., Burban, A., Li, R., Guevel, R. L., Abdel-Razzak, Z., Stieger, B., Guguen-Guillouzo, C., and Guillouzo, A. (2015). Comparative localization and functional activity of the main hepatobiliary transporters in HepaRG cells and primary human hepatocytes. *Toxicol. Sci.* **145**, 157–168.
- Burbank, M. G., Burban, A., Sharanek, A., Weaver, R. J., Guguen-Guillouzo, C., and Guillouzo, A. (2016). Early alterations of bile canaliculi dynamics and the rho kinase/myosin light chain kinase pathway are characteristics of drug-induced intrahepatic cholestasis. *Drug Metab. Dispos.* **44**, 1780–1793.
- Chiang, J. Y. (2009). Bile acids: Regulation of synthesis. *J. Lipid Res.* **50**, 1955–1966.
- Goldring, C., Weaver, R., Kramer, B., Klingmueller, O. A., Van der Water, C. J., Guillouzo, A., et al. (2017). Drug-induced liver injury: mechanism-informed prediction in drug. In *Comprehensive Medicinal Chemistry*, 3rd ed., pp. 1–18. Elsevier, Oxford.
- Guguen-Guillouzo, C., and Guillouzo, A. (2010). General review on in vitro hepatocyte models and their applications. *Methods Mol. Biol.* **640**, 1–40.
- Guo, C., Yang, K., Brouwer, K. R., St Claire, R. L., 3rd., and Brouwer, K. L. (2016). Prediction of altered bile acid disposition due to inhibition of multiple transporters: an integrated approach using sandwich-cultured hepatocytes, mechanistic modeling, and simulation. *J. Pharmacol. Exp. Ther.* **358**, 324–333.
- Hillgren, K. M., Keppler, D., Zur, A. A., Giacomini, K. M., Stieger, B., Cass, C. E., Zhang, L., and International Transporter, C. (2013). Emerging transporters of clinical importance: an update from the International Transporter Consortium. *Clin Pharmacol Ther* **94**, 52–63.
- Jones, H. M., Barton, H. A., Lai, Y., Bi, Y. A., Kimoto, E., Kempshall, S., Tate, S. C., El-Kattan, A., Houston, J. B., Galetin, A., et al. (2012). Mechanistic pharmacokinetic modeling for the prediction of transporter-mediated disposition in humans from sandwich culture human hepatocyte data. *Drug Metab. Dispos.* **40**, 1007–1017.
- Kaschek, D., Mader, W., Fehling-Kaschek, M., Rosenblatt, M., and Timmer, J. (2016). Dynamic modeling, parameter estimation and uncertainty analysis in R. *bioRxiv*. Jan 1: 085001.
- Kreutz, C., Raue, A., Kaschek, D., and Timmer, J. (2013). Profile likelihood in systems biology. *Febs J.* **280**, 2564–2571.
- LeCluyse, E. L., Audus, K. L., and Hochman, J. H. (1994). Formation of extensive canalicular networks by rat hepatocytes cultured in collagen-sandwich configuration. *Am. J. Physiol.* **266**, C1764–C1774.
- Leis, J. R., and Kramer, M. (1988). The simultaneous solution and sensitivity analysis of systems described by ordinary differential equations. *ACM Trans Math Software* **14**, 45–60. *ACM Trans Math Software* **14**, 45–60.
- Li, R., Ghosh, A., Maurer, T. S., Kimoto, E., and Barton, H. A. (2014). Physiologically based pharmacokinetic prediction of telmisartan in human. *Drug Metab. Dispos.* **42**, 1646–1655.
- Liu, X., Brouwer, K. L., Gan, L. S., Brouwer, K. R., Stieger, B., Meier, P. J., Audus, K. L., and LeCluyse, E. L. (1998). Partial maintenance of taurocholate uptake by adult rat hepatocytes cultured in a collagen sandwich configuration. *Pharm. Res.* **15**, 1533–1539.
- Merk, B., Timmer, J., and Kaschek, D. (2015). Higher-order Lie symmetries in identifiability and predictability analysis of dynamic models. *Phys. Rev. E Stat. Nonlin. Soft. Matter Phys.* **92**, 012920.
- Nocedal, J., and Wright, S. (2006). *Numerical Optimization*, 2nd ed. New York: Springer Science & Business Media.
- Pauli-Magnus, C., and Meier, P. J. (2006). Hepatobiliary transporters and drug-induced cholestasis. *Hepatology* **44**, 778–787.
- Raue, A., Kreutz, C., Maiwald, T., Bachmann, J., Schilling, M., Klingmuller, U., and Timmer, J. (2009). Structural and practical identifiability analysis of partially observed dynamical models by exploiting the profile likelihood. *Bioinformatics* **25**, 1923–1929.
- Sharanek, A., Azzi, P. B., Al-Attrache, H., Savary, C. C., Humbert, L., Rainteau, D., Guguen-Guillouzo, C., and Guillouzo, A. (2014). Different dose-dependent mechanisms are involved in early cyclosporine a-induced cholestatic effects in hepaRG cells. *Toxicol. Sci.* **141**, 244–253.
- Sharanek, A., Burban, A., Burbank, M., Le Guevel, R., Li, R., Guillouzo, A., and Guguen-Guillouzo, C. (2016). Rho-kinase/myosin light chain kinase pathway plays a key role in the impairment of bile canaliculi dynamics induced by cholestatic drugs. *Sci. Rep.* **6**, 24709.
- Sharanek, A., Burban, A., Humbert, L., Bachour-El Azzi, P., Felix-Gomes, N., Rainteau, D., and Guillouzo, A. (2015). Cellular accumulation and toxic effects of bile acids in cyclosporine A-treated HepaRG hepatocytes. *Toxicol. Sci.* **147**, 573–587.
- Soetaert, K., Thomas, P., and Woodrow-Setzer, R. (2010). Solving differential equations in R: Package deSolve. Retrieved from *J. Stat. Softw.* **33**, <http://dx.doi.org/10.18637/jss.v033.i09>.
- Swift, B., Pfeifer, N. D., and Brouwer, K. L. (2010). Sandwich-cultured hepatocytes: an in vitro model to evaluate hepatobiliary transporter-based drug interactions and hepatotoxicity. *Drug Metab. Rev.* **42**, 446–471.
- Trauner, M., Meier, P. J., and Boyer, J. L. (1998). Molecular pathogenesis of cholestasis. *N. Engl. J. Med.* **339**, 1217–1227.
- Watanabe, N., Takashimizu, S., Kojima, S., Kagawa, T., Nishizaki, Y., Mine, T., and Matsuzaki, S. (2007). Clinical and pathological features of a prolonged type of acute intrahepatic cholestasis. *Hepatol. Res.* **37**, 598–607.
- Watanabe, N., Tsukada, N., Smith, C., and Phillips, M. (1991). Motility of bile canaliculi in the living animal: implications for bile flow. *J. Cell. Biol.* **113**, 1069–1680.
- Yang, K., Kock, K., Sedykh, A., Tropsha, A., and Brouwer, K. L. (2013). An updated review on drug-induced cholestasis: mechanisms and investigation of physicochemical properties and pharmacokinetic parameters. *J. Pharm Sci* **102**, 3037–3057.
- Yang, K., Pfeifer, N. D., Kock, K., and Brouwer, K. L. (2015). Species differences in hepatobiliary disposition of taurocholic acid in human and rat sandwich-cultured hepatocytes: implications for drug-induced liver injury. *J. Pharmacol. Exp. Ther.* **353**, 415–423.
- Yang, K., Woodhead, J. L., Watkins, P. B., Howell, B. A., and Brouwer, K. L. (2014). Systems pharmacology modeling predicts delayed presentation and species differences in bile acid-mediated troglitazone hepatotoxicity. *Clin. Pharmacol. Ther.* **96**, 589–598.